Ocean Science
Open Access
Discussions

Interactive comment on "The open boundary equation" *by* D. Diederen et al.

M. Toffolon

marco.toffolon@unitn.it

An example of tidal wave propagation in an open channel

An additional reply is useful to address the issues raised by the reviewers (and in particular Referee #2), which we warmly appreciated because they urged us to clarify several elements of our analysis that were not sufficiently clear. Indeed, we are not currently able to formally demonstrate the validity of the Open Boundary Equation (OBE). However, examining in more detail the tidal wave propagation in a specific case is useful to understand the process leading to the establishment of OBE.

Here we report a more detailed example considering an estuary characterized by length $L = 500$ km (with a transmissive boundary condition landward mimicking an

ideal open boundary), tidal amplitude at the mouth $\eta = 2$ m (purely sinusoidal M$_2$ forcing), Strickler coefficient $K = 45$ m$^{1/3}$s^{-1}, width convergence length $b = 100$ km (for exponential variation), horizontal bottom with average depth $h_0 = 10$ m, numerical grid step $\Delta x = 500$ m. Figure 1 shows the geometry of the channel.

The tendency towards the OBE validity is illustrated in Figure 2 for the three equations considered in the manuscript (eqs. 22, 26 and 27). The correlation coefficient tends to unity in a relatively rapid way, while the ratios between the right and left hand sides of the equations follow later, but eventually reach unity as well. The asymptotic tendency suggests that an 'adaptation length' is required to adapt the information imposed by the boundary condition to the OBE (see also the previous reply to Referee #2). Estimating such a length is an open problem, and a work in progress, whose solution might shed a new light on a classical problem. It is clear, however, that there is a process acting towards the establishment of the OBE (see also the hundreds of other numerical runs attached to previous replies by Dirk Diederen), so it is worth examining the features of the tidal wave in different steps of its propagation.

OBE as a tendency towards a progressive wave

Figures 3–8 report the temporal cycle of the tidal wave (water level $\zeta = h - h_0$ and velocity u), of their spatial and temporal derivatives, and of the OBE terms (left and right hand sides of equation 22 in the manuscript), in 6 positions along the estuary (see dots in figure 1). Figure 3 shows what happens at the estuary mouth (where the boundary condition is imposed): the OBE is already approximately valid. The temporal variation of the two sides of the equation ($h_t u_x$ or $\zeta_t u_x$ and $u_t h_x$ or $u_t \zeta_x$, see fourth sub-plot, note that derivatives of h are identical to derivatives of ζ for this case with horizontal bed) is very similar.

In the evaluation of the results, it is also important to consider that numerically evaluated derivatives are affected by errors that are larger than those of the variables,

and that the comparison of products between temporal and spatial derivatives is not straightforward for a two-step method (predictor-corrector) as the MacCormack scheme utilized in this work.

The tendency towards the validity of the OBE becomes even more evident at larger distances (figures 4-8). A small bias (likely due to the numerical evaluation of derivatives mentioned above) remains between the two sides of OBE (fourth sub-plots), but it becomes less important as far as a steep front tends to form, whereby local derivatives become larger. The formation of the steep front, which can eventually evolve in a tidal bore, and the occurrence of another (smaller) peak in the derivatives in the tail of the wave, tend to synchronize the signals for ζ and u and drive the tidal wave propagation towards that of a progressive wave.

Fourier analysis and linearized solution

Referee #2 proposes the linearized wave as a counter-example from which it is implied that OBE is valid only for the case of a phase lag $\phi = 0$. As already discussed in a previous reply, we respectfully disagree with such a counter-example.

Having shown that the OBE tends to be satisfied (at least approximately, if not in a strict formal sense) in the previous figures, we analyze the behaviour of the Fourier series truncated at the first harmonic in figure 9. The first (dominant) harmonic is the one that is usually reproduced by linearized solutions and is typically a good approximation if the amplitude-to-depth ratio is not too large (see, e.g., Toffolon and Savenije, 2011). Figure 9 is interesting because it shows that the 'synchronization' discussed above does not change the phase lag of the first tidal component (see the temporal distance between the two circles), which remains approximately the same in all the six examined locations.

The analysis of figure 9 suggests that it is not the phase lag of the linearized solution

that is important and, consequently, we do not expect that $\phi \to 0$ as implied by Referee #2. Conversely, it is the 'shape' of the wave that allows for the OBE to be satisfied. This remark obviously implies that the OBE is not a 'linear' feature of tidal wave propagation and that any attempt to study it by means of a linearized solution cannot be successful.

The Fourier analysis of the test case was developed for the whole estuary, as well. Figure 10 shows the amplitudes and phases of the first three modes. We note that, after an adjustment length, the amplitudes tend to become constant, reaching a sort of equilibrium state until the effect of the (not exactly transmissive) landward boundary condition is felt. Figure 11 shows the celerities of the first three modes of the tidal waves of ζ (or depth h) and u: also in this case, after a suitable distance all the modes tend to transfer the signal of ζ and u with the same celerity, and this wave speed tends to the well-known $\sqrt{g\,\overline{h}}$ that is characteristic of frictionless prismatic channels. Figure 11c shows that the phase lag u-ζ of the first harmonic remains approximately constant (around 38°), confirming the qualitative observation of figure 9.

The progressive character explained by the Lagreangean interpretation

With the aim of explaining where the progressive character arises, in the following analysis we refer to the description of tidal wave propagation in the Lagrangean framework proposed by Savenije (2012, freely available at www.salinityandtides.com). This analysis also reinforces the relevance of section 5.2 (Lagrangean analysis) within the manuscript.

Some new variables have to be introduced with respect to the manuscript: the Lagrangean velocity V, the actual tidal wave celerity $\widetilde{c}$, the amplification of the tidal velocity amplitude $\delta_u = (1/u)\,\partial u/\partial x$. It is further assumed that the Lagrangean function describing the wave can be approached by a sinus; note that the resulting Eulerian wave is not sinusoidal.

By using the relationship (Savenije, 2012)

$$\frac{\partial u}{\partial x} = -\frac{1}{\widetilde{c}}\frac{dV}{dt} + \delta_u V \,, \tag{1}$$

the Eulerian water balance

$$\frac{\partial h}{\partial t} + u\frac{\partial h}{\partial x} + h\frac{\partial u}{\partial x} - \frac{hu}{b} = 0 \tag{2}$$

can be written in Lagrangean terms as

$$\frac{dh}{dt} = \frac{h}{\widetilde{c}}\frac{dV}{dt} + hV\beta' \tag{3}$$

where

$$\beta' = \frac{1}{b} - \delta_u \tag{4}$$

is related to β in the manuscript, but accounts also for the Lagrangean damping of velocity.

Recalling that $dx = V dt$ in the Lagrangean framework, it is possible to rewrite (3) as

$$\frac{dh}{h} = \frac{1}{\widetilde{c}}dV + \beta' dx \,, \tag{5}$$

and integrate it from low water slack (LWS) to a generic state (with velocity V and distance S from the starting point). This leads to

$$\frac{h}{h_{LWS}} = \exp(\beta' S)\,\exp\left(\frac{V}{\widetilde{c}}\right), \tag{6}$$

or

$$\frac{h'_p}{h_{LWS}} = \exp\left(\frac{V}{\widetilde{c}}\right) \simeq 1 + \frac{V}{\widetilde{c}} \,, \tag{7}$$

C562

where

$$h'_p = h\exp(-\beta' S)\,. \tag{8}$$

Note that h'_p is the transformed water depth that reflects the Lagrangean deformation due to convergence and tidal damping, and is not exactly the same quantity as h_p in the manuscript. Moreover, the latter approximate equality of equation (7) relies on the fact that the Froude number $V/\widetilde{c}$ is typically small in tidal flows. Therefore, it directly follows from equation (7) that

$$z_p = h'_p - h_{LWS} \simeq \frac{h_{LWS}}{\widetilde{c}}\,V \,, \tag{9}$$

where z_p is the variation of the transformed Lagrangean water level referred to the water level at LWS.

If we consider the ellipses for water level and velocity against the distance S travelled by an actual water particle (Lagrangean approach, as in Figure 7 of the manuscript), equation (9) implies that the tidal ellipse of the transformed Lagrangean water level (z_p) is completely in phase with (and proportional to) the ellipse of the Lagrangean velocity V.

We can also explicitly analyze an example using the test case discussed above. Figure 12 shows the Eulerian variables and their Lagrangean counterparts (water level Z and velocity V) reconstructed starting from $\zeta_{LWS} = h_{LWS} - h_0$ in $x = 100$ km. Figure 13 shows the ellipses: focusing on the third plot, we see that the actual water level Z is inclined (hence not in phase with velocity V), while the transformed variable z_p is put in phase with V by accounting for the Lagrangean rise ($h_{LWS}\exp(\beta' S) - h_0$). Finally, figure 14 directly shows that the transformed variable z_p is highly linearly correlated with the velocity, and the proportionality constant is indeed given by $h_{LWS}/\widetilde{c}$ as predicted by equation (9). This further corroborates that, in the Lagrangean framework, the wave travels as a progressive wave.

Interestingly, the fact that the transformed Lagrangean wave travels as a progressive wave is caused essentially by the water balance equation, which explains why it also works for estuaries with friction. The only influence from the momentum equation is through the wave celerity and the assumed sinusoidal shape, which might explain the small deviations noted in Figure 14.

The open boundary approximation

As a final consideration, it is important to remind that the open boundary is an idealization for the infinite channel case, which does not exist in reality. However, such a conceptual scheme can be satisfactorily used in many cases of long estuaries, in particular if there are no elements that can produce strong reflections of the wave, or if there is convergence that dampens out the reflected wave.

References

Savenije, H. H. G.: *Salinity and Tides in Alluvial Estuaries, 2nd revised edn.*, available at: www.salinityandtides.com, Delft, the Netherlands, 2012.

Toffolon, M. and Savenije, H. H. G.: Revisiting linearized one-dimensional tidal propagation, *J. Geophys. Res., 116*, C07007, doi:10.1029/2010JC006616, 2011.

Interactive comment on Ocean Sci. Discuss., 12, 925, 2015.

C564
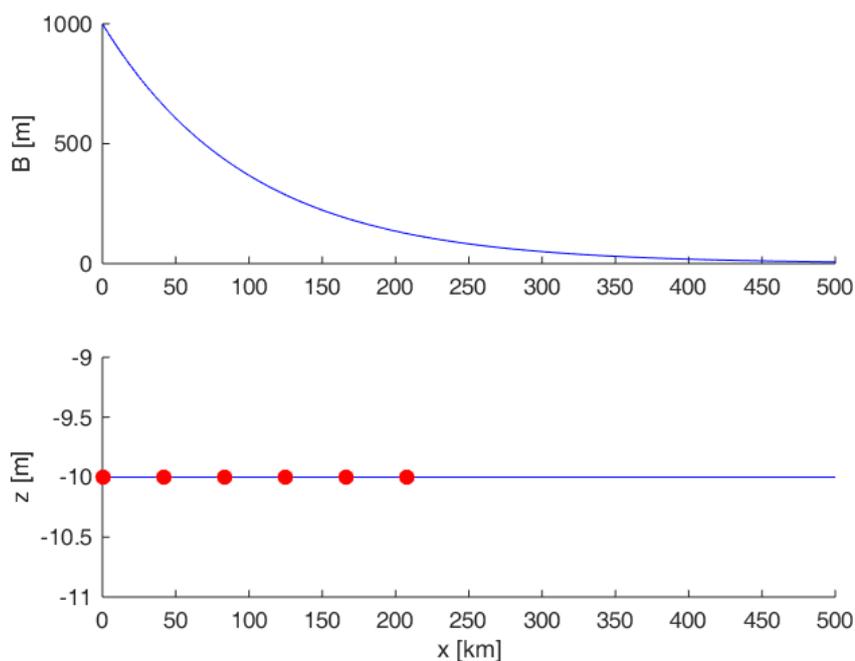
Fig. 1. Longitudinal profiles of width and bottom. Dots indicates the locations where the temporal behaviour is shown in figures 3-8.
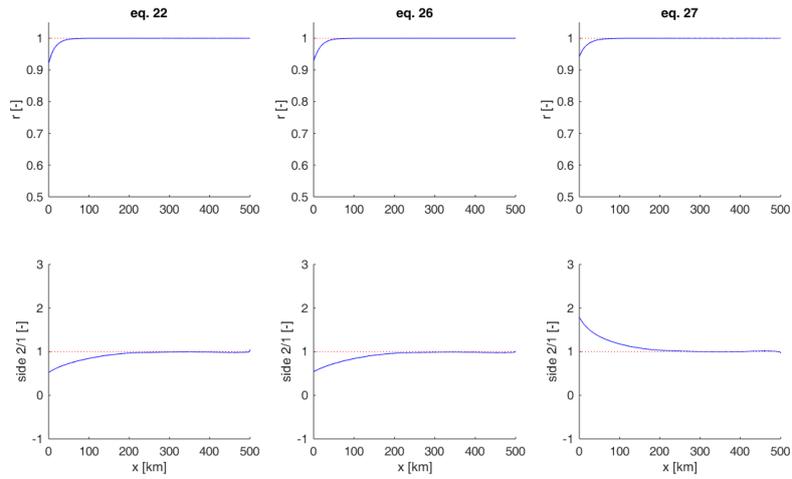
Fig. 2. Longitudinal variation of the correlation coefficient (first row) and of the ratio between right hand side and left hand side of equations 22, 26 and 27 in the manuscript.

C566
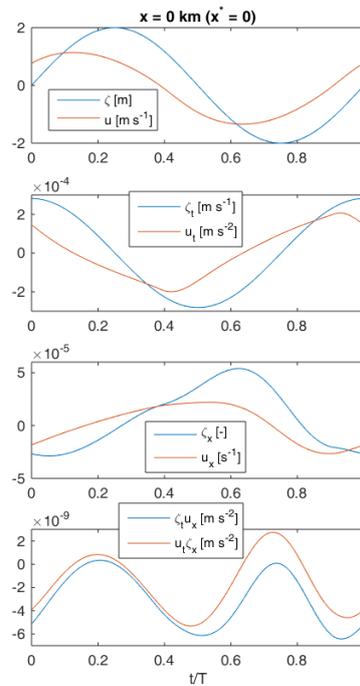
Fig. 3. Temporal variation of ζ and u (first plot), ζ_t and u_t (second plot), ζ_x and u_x (third plot), and $\zeta_t \, u_x$ and $u_t \, \zeta_x$ (fourth plot) in $x=0$ km.

C567
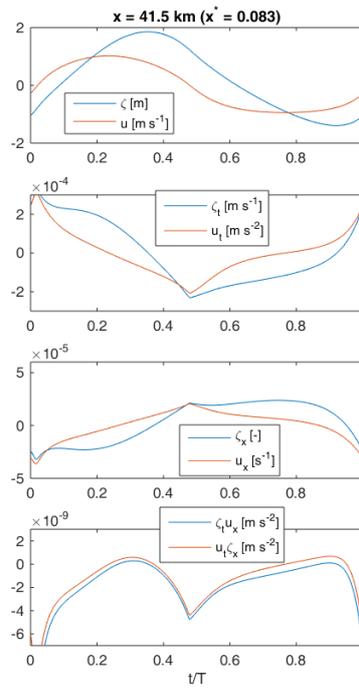
Fig. 4. Temporal variation of ζ and u (first plot), ζ_t and u_t (second plot), ζ_x and u_x (third plot), and $\zeta_t \, u_x$ and $u_t \, \zeta_x$ (fourth plot) in $x=41.5$ km.

C568
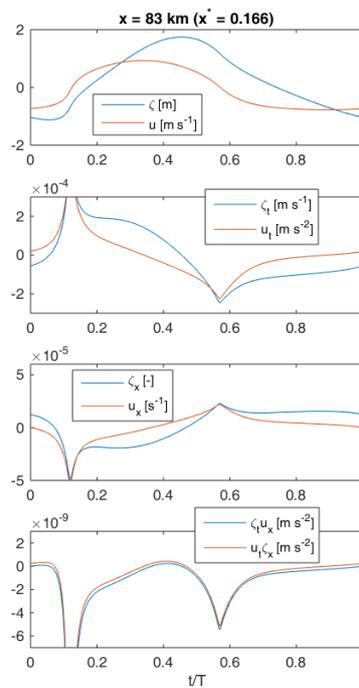
Fig. 5. Temporal variation of ζ and u (first plot), ζ_t and u_t (second plot), ζ_x and u_x (third plot), and $\zeta_t \, u_x$ and $u_t \, \zeta_x$ (fourth plot) in $x=83$ km.

C569
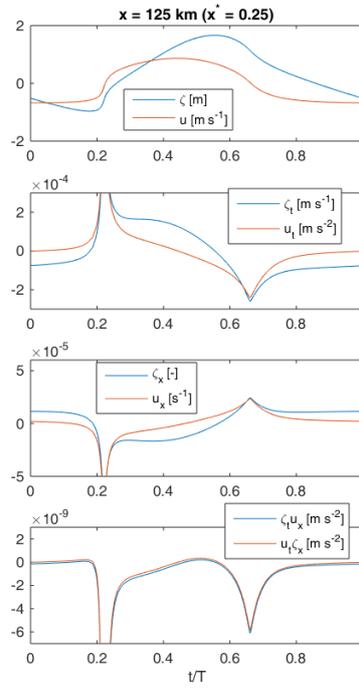
Fig. 6. Temporal variation of ζ and u (first plot), ζ_t and u_t (second plot), ζ_x and u_x (third plot), and $\zeta_t \, u_x$ and $u_t \, \zeta_x$ (fourth plot) in $x=125$ km.
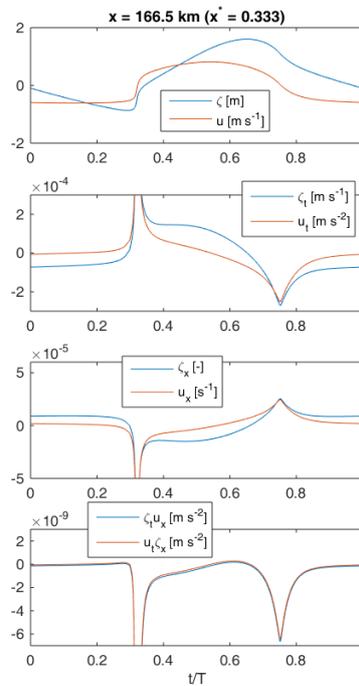
Fig. 7. Temporal variation of ζ and u (first plot), ζ_t and u_t (second plot), ζ_x and u_x (third plot), and $\zeta_t \, u_x$ and $u_t \, \zeta_x$ (fourth plot) in $x=166.5$ km.
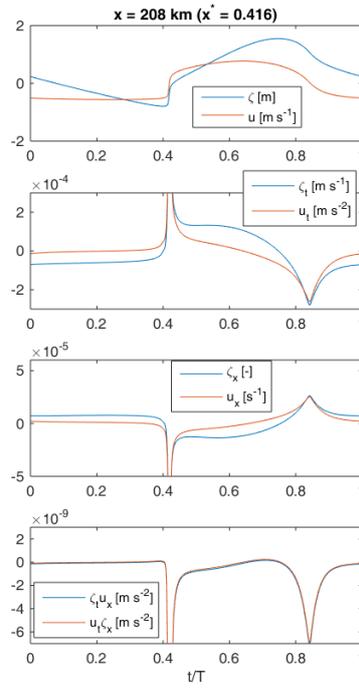
Fig. 8. Temporal variation of ζ and u (first plot), ζ_t and u_t (second plot), ζ_x and u_x (third plot), and $\zeta_t \, u_x$ and $u_t \, \zeta_x$ (fourth plot) in $x=208$ km.
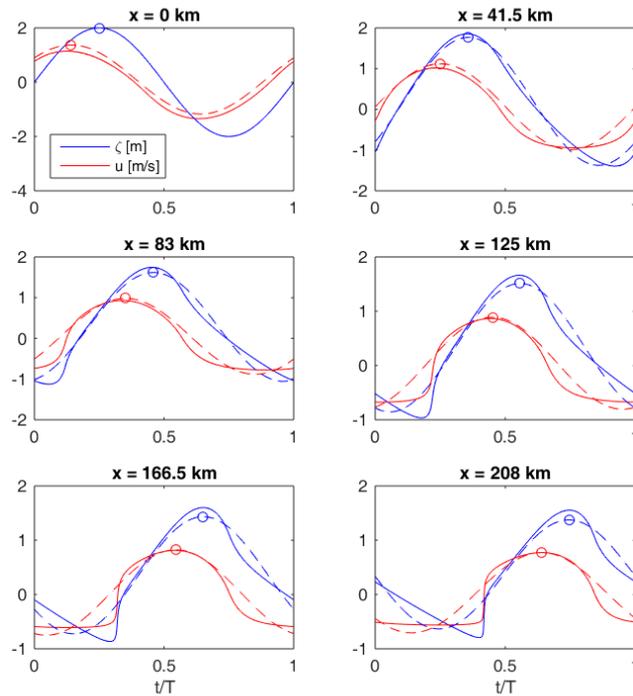
Fig. 9. Tidal waves and Fourier series truncated at the first harmonic. Circles indicate the maxima of the dominant tidal component, from which it is possible to detect the phase lag u-ζ.
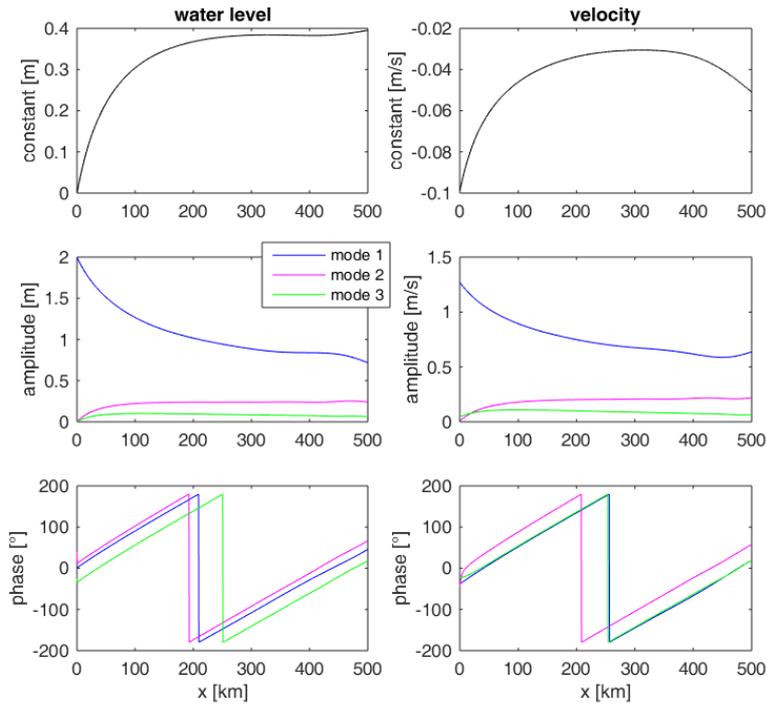
Fig. 10. Fourier analysis of tidal wave. From top to bottom: constant term, amplitudes, phases of first three modes. Left column: water level ζ; right column: velocity u.
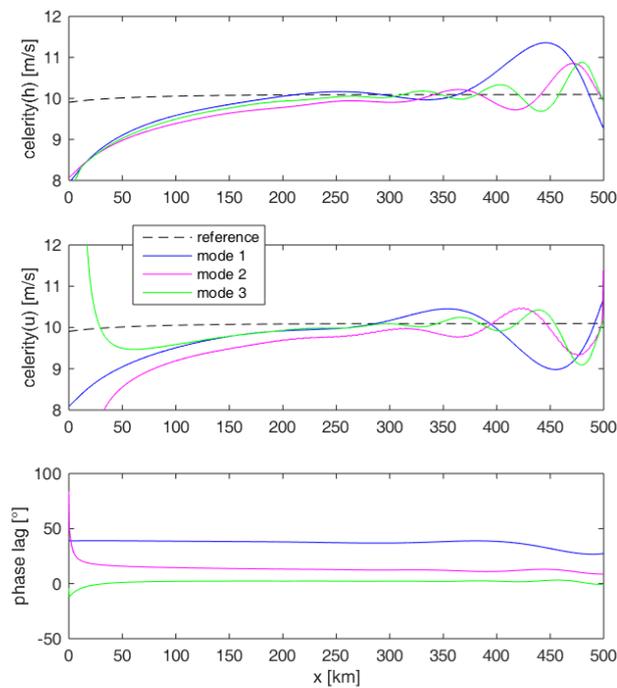
**Fig. 11.** Wave celerity for water level ζ, for velocity u, phase lag u-ζ. Colors refer to the first three modes; black dashed line to wave celerity in a frictionless prismatic channel.
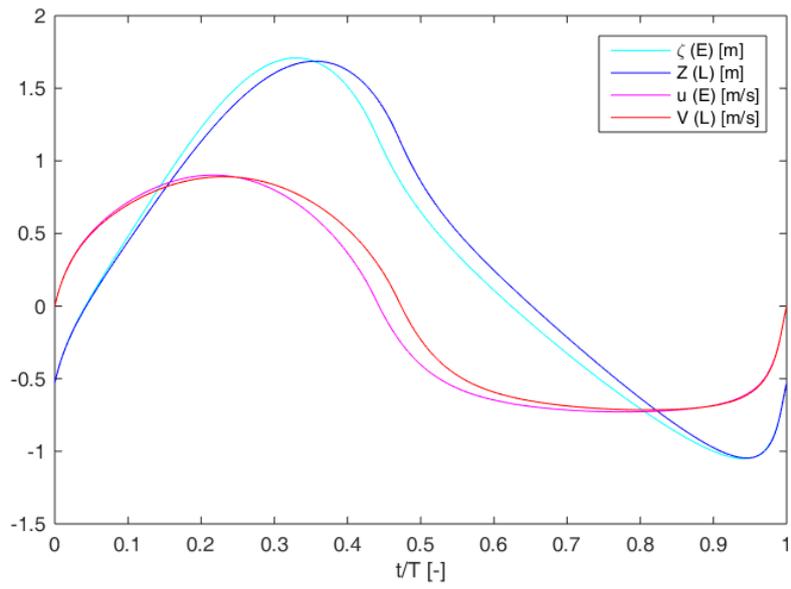
Fig. 12. Lagrangean water level Z and velocity V compared with Eulerian values ζ and u in $x=100$ km.
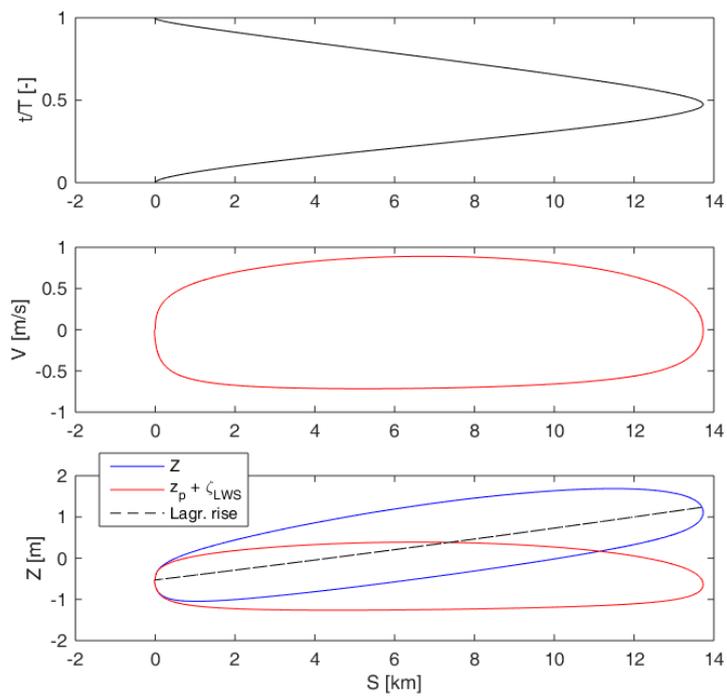
Fig. 13. Lagrangean displacement S in time (first plot) and ellipses V-S (second plot) and Z-S (third plot).
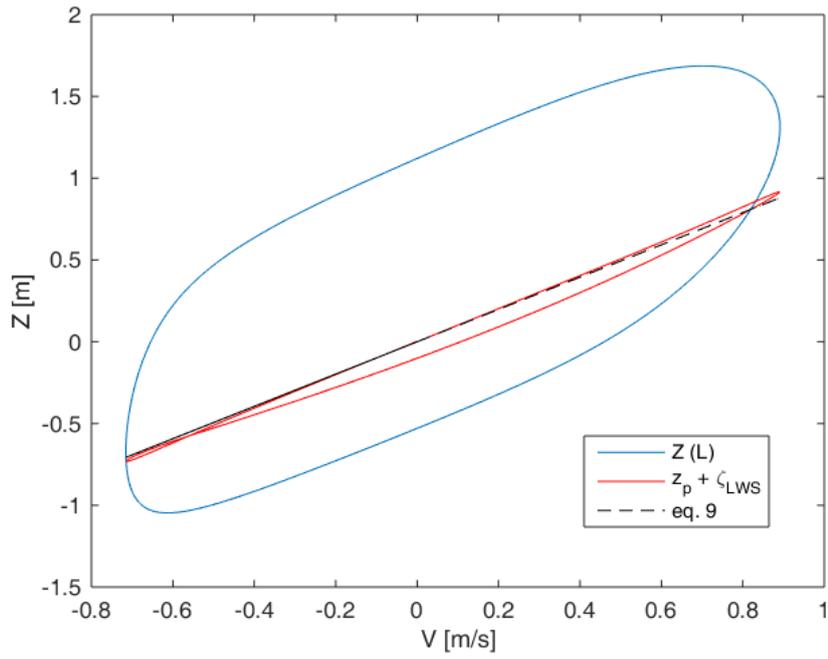
Fig. 14. Lagrangean water level against velocity V: Z is the actual value, $z_p + \zeta_{LWS}$ is the transformed water level. Black dashed lines: equation (9).

C578